

Hydrography within the Central and East Basins of the Bransfield Strait, Antarctica

CARA WILSON,* GARY P. KLICKHAMMER, AND CAROL S. CHIN

College of Oceanic and Atmospheric Sciences, Oregon State University, Corvallis, Oregon

(Manuscript received 27 June 1997, in final form 2 April 1998)

ABSTRACT

The hydrography in the central and east basins of the Bransfield Strait is examined using data collected along a track 340 km long through the strait in November 1995, in conjunction with historical data from the NODC database. Circumpolar Deep Water (CDW) was seen throughout most of the central basin and the western east basin, in contrast to earlier studies that have shown CDW being absent or only weakly present in the strait. In the western part of the central basin the CDW was present as a narrow band near Deception Island with strong thermal gradients at its southern boundary, consistent with previous observations. Local deep-water formation produces bottom waters in the central and east basins that are distinct from one another and distinct from the surrounding deep waters outside the strait. The east basin has a more complex stratification than the central basin that must be the result of multiple sources. A model presented here explains the deep water in the east basin as a mixture between the sill waters and deep waters from both the central basin and the Weddell Sea. Weddell Sea sill water is the predominate end-member. Analysis of the historic data shows that temperature and salinity within the central and east basins of the Bransfield have varied considerably over the past 30 years. A systematic change in the slope of the T - S relation in the central basin is observed, the result of the middepth water becoming colder and fresher. The east basin has also become colder and fresher over the past 30 years; however, this change has occurred uniformly throughout the water column without affecting the slope of the east basin T - S relation. The changes in the east basin have been sporadic, with the largest change occurring between 1963 and 1975.

1. Introduction

The Bransfield Strait is located between the northern tip of the Antarctica Peninsula and the South Shetland Islands (Fig. 1). Active volcanism in this back-arc rift has been documented on Deception Island (Baker et al. 1969; Baker and McReath 1971; Orheim 1972; Elderfield 1972). Young (<3000 to 300 000 yr) volcanism is also found on King George Island (Birkenmajer and Keller 1990) and submerged volcanism occurs along the rift (Keller et al. 1992). Elevated levels of ^3He observed within the east basin and the eastern central basin (Schlosser et al. 1988; Chin et al. 1996) have suggested that this region is hydrothermally active, as have sediments showing hydrothermal alteration (Brault and Simoneit 1990; Whiticar and Suess 1990).

The strait comprises three separate basins that are isolated from the surrounding ocean by relatively shallow

sills, shown in Fig. 2a. Local deep-water formation results in different water characteristics in each of the separate basins, a phenomena that has attracted the attention of oceanographers since the early 1900s (Clowes 1934). Because the deep water formed in the Bransfield Strait cannot leave the basins due to topographical restraints, this area is well suited to examine aspects of deep-water formation and temporal variability.

The Bransfield Strait has an important impact on Antarctica biological processes as it is a breeding ground for the krill, *Euphausia superba* (Capella et al. 1992a). The life cycle of *E. superba* involves a descent-ascent pattern in which embryos can sink to depths greater than 2000 m and ascend back up through the water column after hatching into larvae. Because the temperatures encountered by the embryos affect their hatching potential (Hofmann et al. 1992), understanding the biological dynamics within this area requires knowledge of the physical environment, in particular the distribution of Circumpolar Deep Water. Several international programs, for example, BIOMASS, FIBEX, SIBEX, and RACER (Sievers 1982; Grelowski and Tokarczyk 1985; Huntley et al. 1991), have focused on the biological and physical dynamics within the strait.

However, published work on the hydrography of the Bransfield Strait remains sparse. The work by Clowes (1934) remains the most comprehensive study in both

* Current affiliation: InterRidge Office, Laboratoire de Pétrologie, Université Pierre et Marie Curie, Paris, France.

Corresponding author address: Dr. Cara Wilson, InterRidge Office, Laboratoire de Pétrologie, Université Pierre et Marie Curie, 4 Place Jussieu, Tour 26, 3ème étage, 75252 Paris Cedex 05, France.
E-mail: wilson@ccr.jussieu.fr

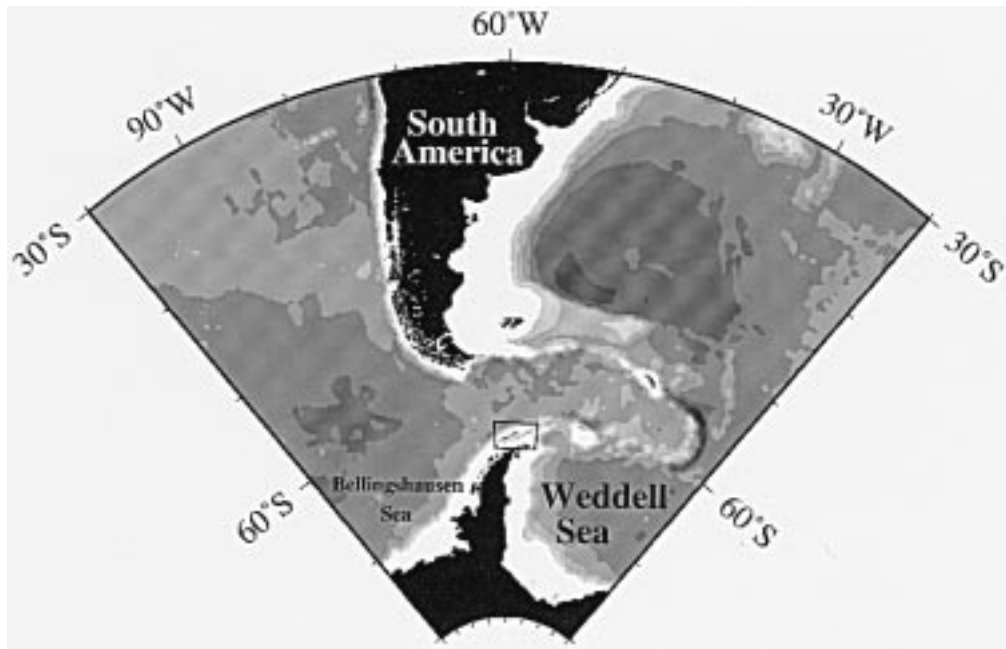


FIG. 1. Map showing the location of the Bransfield Strait, outlined by the box, between the Antarctic Peninsula and the South Shetland Islands.

spatial and temporal extent, although its vertical resolution is limited due to the measuring techniques at that time. The relatively more recent hydrographic study by Gordon and Nowlin (1978), while having a better vertical resolution, consisted of only five stations within the strait. Whitworth et al. (1994) and Hofmann et al. (1996) both analyzed historic compilations of data in the strait and surrounding areas. However, they mainly focused on the differences between the Bransfield Strait and the adjacent waters and did not discuss differences within the strait. The biologically motivated studies have either concentrated on the upper water column (0–500 m) (Sievers 1982; Grelowski and Tokarczyk 1985; Huntley et al. 1991; Niiler et al. 1991) or on coastal areas (Capella et al. 1992b).

This paper presents hydrographic data from a survey looking for hydrothermal activity within the central and east Bransfield basins (Chin et al. 1996) by the RVIB *N. B. Palmer* in October–November 1995. These data, in conjunction with historic National Oceanic Data Center (NODC) data, are used to examine the distribution of Circumpolar Deep Water (CDW) within the Bransfield and to analyze the deep water of the central and east basins. A model is presented that explains the complex structure of the east basin as the result of a four end-member mixing process. The temporal variability of the central and east basin deep water is examined for the period between 1963 and 1995.

2. Geographic description

The Bransfield Strait is roughly 120 km wide and extends 460 km from Clarence Island in the northeast

to Low Island in the southwest (Fig. 2a). It is composed of three basins, most commonly referred to as the west, central, and east basins. The basins deepen to the northeast, having a maximum axial depth in the west basin of 1100 m near Low Island and a maximum depth of 2700 m in the east basin south of Elephant Island. Sills shallower than 500 m (shaded white on Fig. 2a) almost entirely encircle the strait, restricting the inflow of deep water from the adjacent Drake Passage and Weddell Sea. The east basin has the deepest access to outside water with sills deeper than 500 m around Clarence Island and northeast of the tip of the Antarctic Peninsula. In contrast, there are no passages deeper than 500 m into either the central or west basin. A passage of 400 m occurs in the southwest between Smith and Snow Islands, and one of 500 m between King George and Elephant Islands in the northeast. The central basin is isolated from the adjacent basins by sills of 1000 and 1100 m at its western and eastern boundaries.

Also shown in Fig. 2a are the station locations from the RVIB *N. B. Palmer* cruise. Due to time constraints only the central and east basins were sampled. The main objective of the cruise was to systematically survey the strait for indications of hydrothermal activity (Chin et al. 1996). For this reason the station locations follow an intermittent ridge, which transects the strait in a line extending from Deception Island to Clarence Island. While this ridge system is not evident in the bathymetry shown in Fig. 2, it is readily visible in high-resolution multibeam bathymetry (Gràcia et al. 1996; Lawver et al. 1996). The central and east basins have significantly

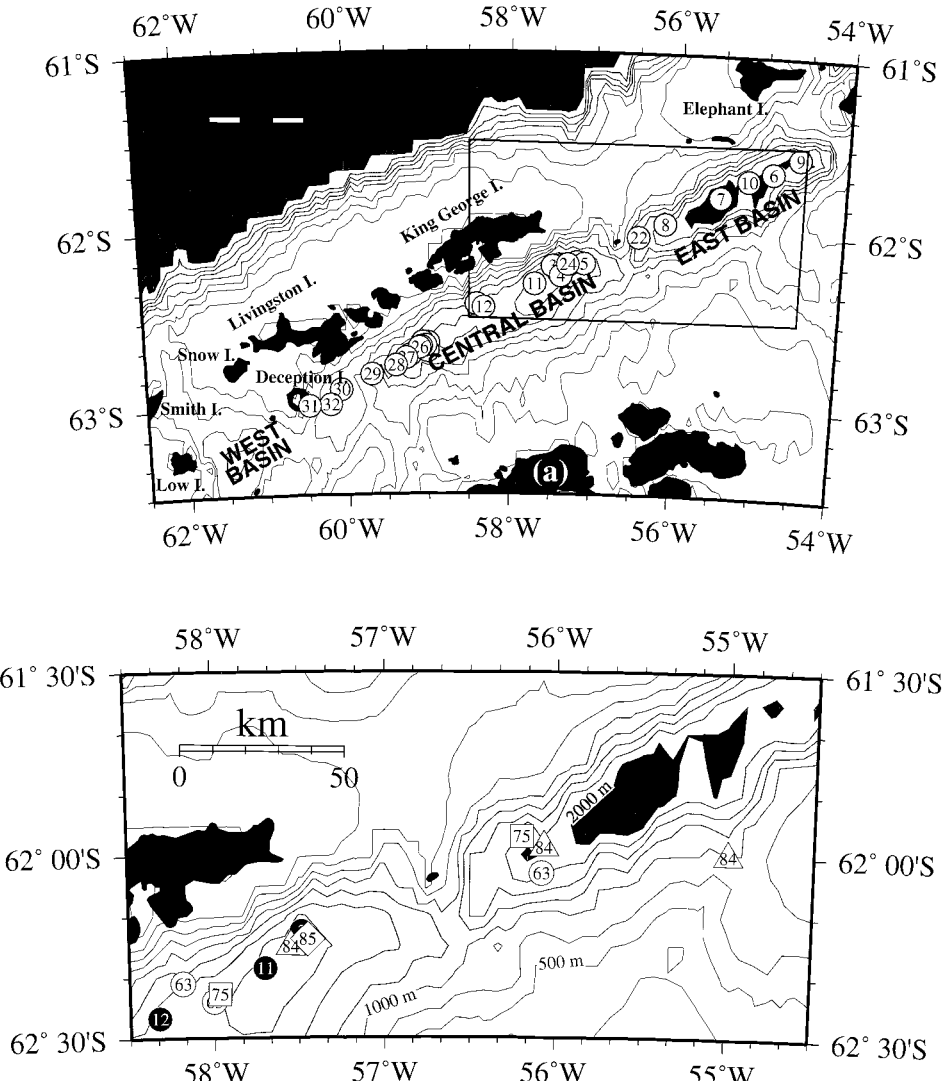


FIG. 2. Map showing bathymetry (ETOPO5) of the Bransfield Strait and station locations of (a) the 1995 *Palmer* data and (b) the historical data. The boxed area in (a) represents the region shown in (b). The symbols in (b) represent locations of the historic data from 1963 (white circles), 1975 (squares), 1984 (triangles), 1985 (diamond), and three stations from 1995 (black circles); SL3 is partially visible behind the 1984 and 1985 stations in the central basin. The contour interval for both maps is 250 m. The scale shading changes at 500, 1000, and 2000 m. With the exception of the east basin, sills shallower than 500 m (shown in white) isolate the waters in the Bransfield Strait from outside waters.

different topography. The central basin is characterized by a fairly smooth bottom bathymetry, marred only by the ridges which do not span the width of the basin. In contrast, the narrower east basin is broken up into three separate subbasins that are isolated from one another below ~ 2000 m (L. Lawver 1995, personal communication).

3. Circumpolar Deep Water

The Circumpolar Deep Water (CDW) is one of the most prominent water masses of the Southern Ocean.

Within the Antarctic Circumpolar Current it has been subdivided into the upper CDW (UCDW), characterized by nutrient and temperature (2°C) maxima and an oxygen minimum found near 500 m, and the lower CDW (LCDW), characterized by a salinity maximum centered near 700 m (Gordon 1967). Near Antarctica, northward Ekman transport of surface water results in the CDW upwelling closer to the surface. The resulting modified CDW is not divided into upper and lower parts. Although this modified CDW originates from the LCDW (Whitworth et al. 1994), it has both a temperature and a salinity maxima that occur concurrently.

The modified CDW (hereafter referred to as CDW) in the Bransfield Strait is centered at 300–400 m and rarely reaches temperatures $>0.5^{\circ}\text{C}$ (Clowes 1934; Capella et al. 1992b). The CDW is usually absent or only weakly present within the strait (Clowes 1934; Gordon and Nowlin 1978). In general, it is usually found in the western portion of the strait near its entrance point between Smith and Snow Islands (Clowes 1934; Niiler et al. 1991; Capella et al. 1992b), and along the southern coast of the South Shetland Islands (Capella et al. 1992b; Hofmann et al. 1996).

The spatial distribution of CDW around the Bransfield Strait area is seen in the temperature maximum below 150 m from the NODC data, shown in Fig. 3a. This dataset encompasses measurements from 1926 to 1990 and represents a seasonal and annual average. Outside of the strait the CDW is clearly visible as the water $>1^{\circ}\text{C}$ north of the South Shetland Islands, while within the strait the maximum temperatures are $<0.5^{\circ}\text{C}$. The warmest temperatures, between 0.0° and 0.5°C , are found along the southern coast of the South Shetland Islands. The shoaling of the CDW south of Drake Passage is evident in the transition of the temperature maximum from a depth of 400–500 m north of the South Shetland islands to around 200–300 m in the strait (Fig. 3b).

Sections of potential temperature, salinity, and potential density through the central and east basins from the *Palmer* cruise are shown in Fig. 4. The CDW is present throughout the central basin, as seen by the prominent subsurface temperature maximum centered on the $\sigma_0 = 27.7$ isopycnal (the white line in Fig. 4a). This distribution is in contrast to previous studies that described a weak CDW within the strait (Clowes 1934; Gordon and Nowlin 1978), or which only observed CDW along the southern flank of the South Shetland Islands (Capella et al. 1992b; Hofmann et al. 1996). In 1995 the CDW appeared the strongest in two locations: the westernmost part of the central basin (SL31) and over the sill between the central and east basins, where it appeared bifurcated. The CDW was absent in the eastern east basin (SL7, SL10, SL6, and SL9). The CDW can also be seen in the salinity distribution (Fig. 4b). However, the salinity maximum is not as developed as the temperature maximum and does not extend continuously across the central basin.

The strong CDW signal seen at SL31, the mouth of Deception Island, is consistent with previous descriptions of the CDW entering the strait west of Snow Island (Clowes 1934; Niiler et al. 1991; Capella et al. 1992b). Directly east of SL31, the CDW strength decreases considerably (SL29, SL30, and SL32). In the 15 km between SL31 and SL32, the temperature maximum of 0.6°C at 300 m decreases more than 2°C to a local minimum -1.5°C at SL32. Niiler et al. (1991) observed a similar front in this area, having vertical isotherms at 200 m that changed from -0.1° to -0.7°C over 20 km. These sharp thermal gradients result from the CDW

flowing into the Bransfield strait in a narrow tongue circling Deception Island (Capella 1992b).

The subsurface temperature maximum between 56° and 57°W (Fig. 4) is interesting as CDW has usually been absent in this part of the strait. However, previous studies have shown some signs of CDW in the eastern central basin. For example, the horizontal contours in Capella (1992b) reveal an intrusion of warm water between King George Island and Elephant Island, although it does not appear to penetrate into the central or east basins. The sections of Gordon and Nowlin (1978) show an interleaving of warm water and a salinity maximum at 400-m depth at station 60, the eastern side of the central basin. Additionally, sections across the central basin (north–south) in November 1929 had temperature maxima in the eastern central basin (Clowes 1934).

There are three possible explanations for the presence of CDW in the eastern Bransfield Strait. It could be an eddy of CDW formed in the western strait and advected eastward (Gordon and Nowlin 1978). Alternatively, it could be part of the topographically controlled current of CDW flowing south of the Shetland Islands (Capella et al. 1992b) that meandered into the middle of the strait. Last, the CDW could have entered the strait between King George Island and Elephant Island, a wider entrance than the narrow passage between Smith and Snow Islands (see Fig. 2a). Without additional data from the continental shelf region it is impossible to determine the pathway of the CDW into the eastern Bransfield Strait. The important thing to note is that in contrast to the paradigm, CDW is sometimes present within the Bransfield Strait and displays significant variability from year to year.

4. Deep water structure

The deep waters of the east and central basins are significantly different from one another. Central basin bottom water is colder and denser, reaching a minimum potential temperature of -1.76°C at $\sigma_4 = 46.28$. This water is colder and denser than Weddell Sea bottom water (-1.2°C and $\sigma_4 = 46.25$), which is often described as the coldest and densest bottom water in the Southern Ocean (Carmack 1977). Although the east basin is roughly 500 m deeper than the central basin, its bottom waters are warmer by $\sim 0.5^{\circ}\text{C}$ and fresher by 0.4. The east basin is also more homogeneous than the central basin, having a nearly uniform salinity below 1000 m.

The bottom water in the central and east basins is more than 1°C colder and 0.08 fresher relative to water at the same depth outside the strait in the Weddell Sea. The absence outside the strait of water with similar temperature and salinity indicates that Bransfield bottom waters are formed locally within the strait (Clowes 1934; Gordon and Nowlin 1978; Killworth 1983), although it is uncertain whether this process occurs by deep convection (Killworth 1983) or by shelf brine ejection.

Gordon and Nowlin (1978) suggested that winter

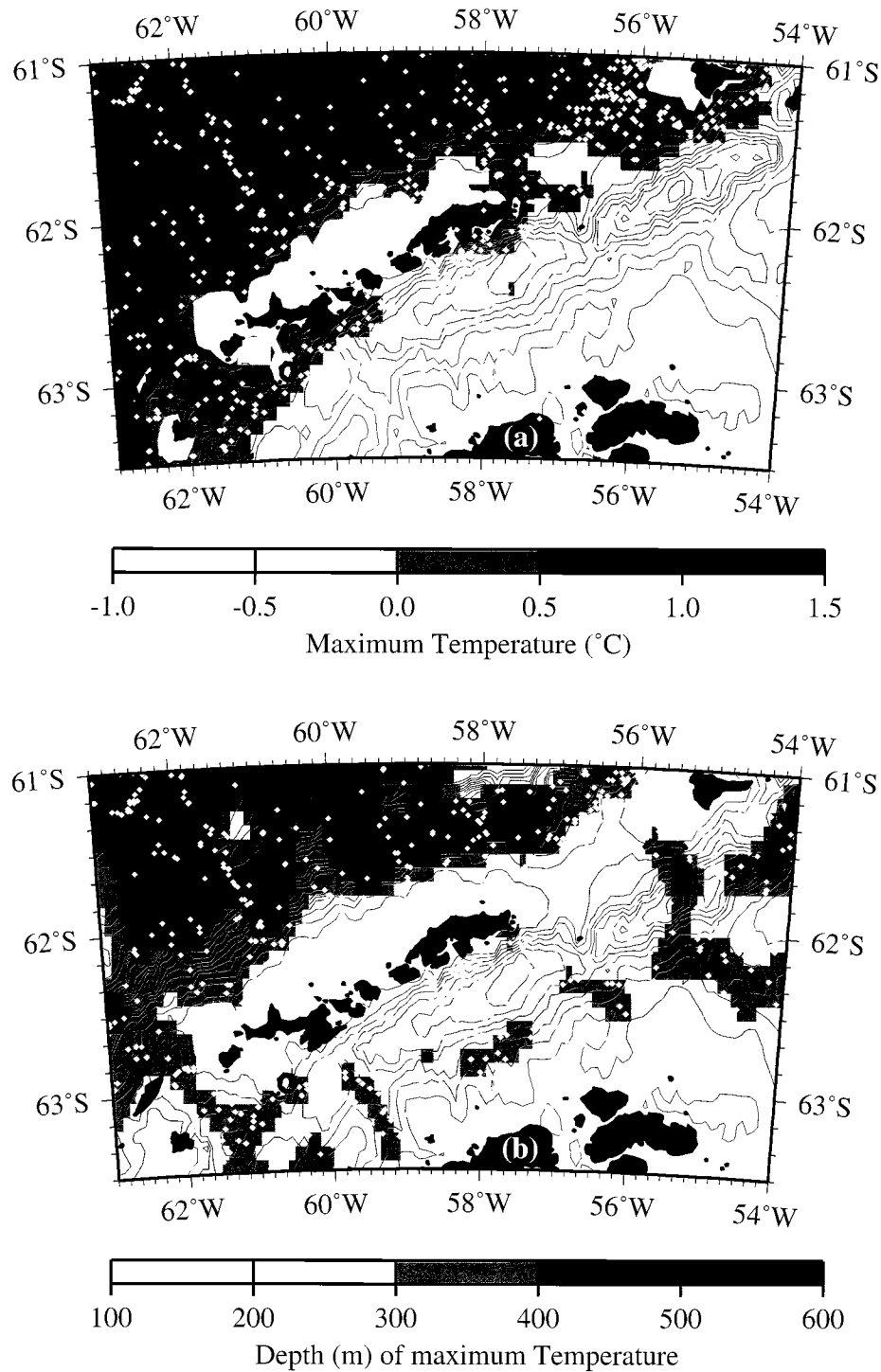


FIG. 3. Distribution of (a) the temperature maximum below 150 m and (b) the depth of the temperature maximum from the NODC dataset. This dataset encompasses data from 1926 to 1990 and represents a seasonal and annual average. Circumpolar Deep Water (CDW) is visible as the water $>1^{\circ}\text{C}$ north of the South Shetland Islands and within the Bransfield as the water $>0.0^{\circ}\text{C}$ along the south flanks of the South Shetland Islands. Both distributions are overlaid on the bathymetry contoured at 250 m; areas in white are less than 150 m deep. Data points are indicated by the white dots.

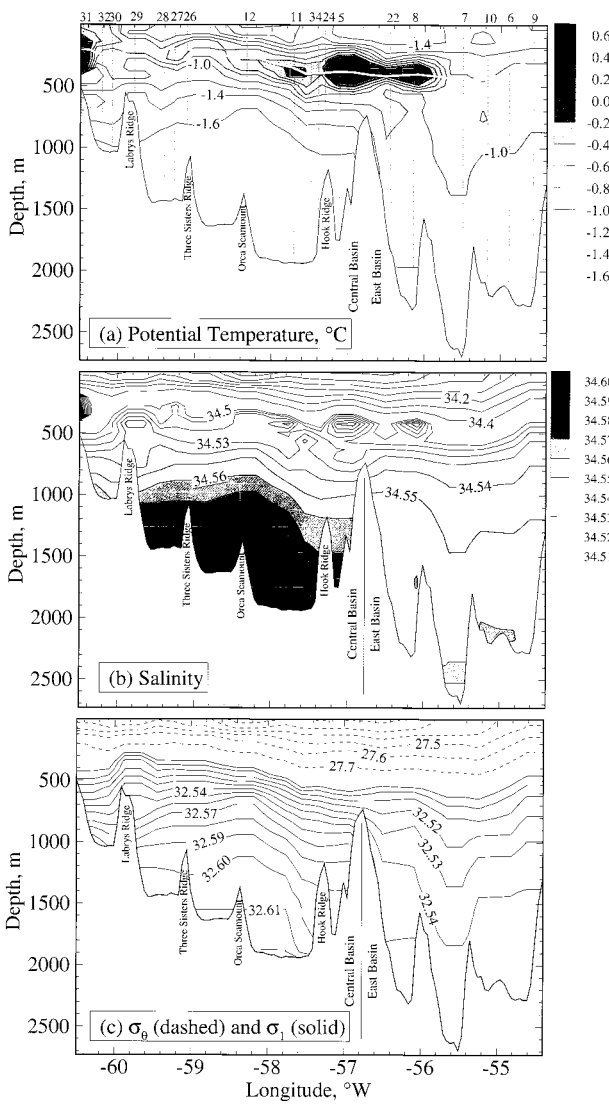


FIG. 4. Contours of (a) potential temperature, (b) salinity, and (c) potential density within the central and east basins. The white line in (a) is the $\sigma_0 = 27.7$ isopycnal. The bathymetry is taken from Seabeam data collected during the cruise. The labeled topographic highs in the central basin are part of the ridge system and do not isolate the water masses within the basin. In contrast, the sills between the central and east basin, and the topographic highs within the east basin, isolate the waters to either side.

shelf water formed on the northern tip of the Antarctic Peninsula creates the deep water within Bransfield Strait. Extrapolating the T - S properties of deep east basin water to freezing temperatures, they suggested that a winter shelf water with a salinity of 34.62 psu forms the observed Bransfield bottom water. While this shelf water would also be a source for deep water outside of the strait, they surmised that the absence of warm, salty CDW in the strait results in the colder fresher Bransfield water. However, CDW is not always absent in the strait, as discussed in the previous section.

An alternative hypothesis was put forth by Whitworth et al. (1994). They concluded that deep Bransfield water is a mixture of Weddell Sea water, Antarctic Circumpolar Current water, and northwest Weddell Sea shelf water, which is advected northward and sinks isopycnally. This process can occur year-round and removes the need to infer a winter shelf component to produce the observed bottom water. By this hypothesis Bransfield bottom water has the same source as Weddell Sea and Scotia Sea deep water, but with a higher shelf water component.

However, neither of these explanations addresses the variation between the deep waters of the central and east basins of the Bransfield Strait. Clearly, there must be multiple sources that lead to the differentiation of the bottom waters of these two adjacent basins. Gordon and Nowlin (1978) touched on this problem; citing more complex stratification in the central basin relative to the east basin, they surmised that additional, unknown, processes contribute to the formation of central basin deep water. Here the temperature–salinity distribution within the deep central and east basins is examined in an attempt to resolve this issue.

The T - S diagram for all of the *Palmer* data is shown in Fig. 5. The data have been separated into three different regional categories: the westernmost part of the central basin (Fig. 5a), the rest of the central basin (Fig. 5b), and the east basin (Fig. 5c). The westernmost part of the central basin is distinguishable from the rest of the basin by its higher surface temperature due to the influence of the adjacent Bellingshausen Sea. For comparison, surface water T - S from the Bellingshausen Sea (Read et al. 1995) is shown as the irregularly shaped gray area. The subsurface temperature maximum, indicative of CDW, is present throughout all three domains with a maximum of 0.5°C at $\sigma_0 = 27.74$. The front marking the edge of the CDW near SL31 is evident in the separation of data below $\sigma_0 = 27.6$ in Fig. 5a.

a. Central basin

Figure 6 is a more detailed view of the data within the gray boxed area in Fig. 5. An upper temperature of -1°C was chosen so as to include deep east basin data; however, it should be noted that this isotherm, reaching 1400 m in the east basin, shoals to nearly 300 m in the western central basin (see Fig. 4a). There are two types of T - S curves from the central basin: one with a fairly tight relationship (black) and one with a more complicated relationship that is considerably warmer and saltier (shown in gray).

The warmer, saltier curves are found in either the western central basin (SL28–32) or the eastern central basin (SL3, SL23, and SL24). The eastern inhomogeneities lie above the $\sigma_1 = 32.56$ isopycnal, which is at about 1000 m, the depth of the sill between the central and the east basins. Below the sill depth the central basin data converge into one T - S curve. However, two distinct

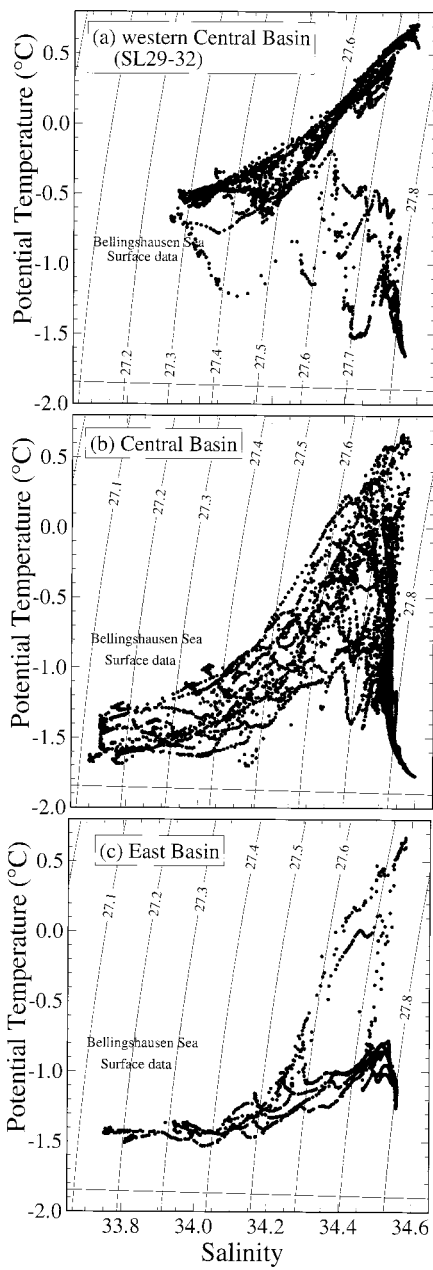


FIG. 5. Potential temperature–salinity diagrams for all stations within (a) the western central basin, (b) the central basin, and (c) the east basin. Lines of constant σ_0 are drawn on the plot. The gray irregular shaped area represents the T – S properties of surface water (in November) from the Bellingshausen Sea, taken from Read et al. (1995). The line at the bottom of the plot indicates the freezing point. The gray box outlines the region shown in Fig. 6.

types of depth profiles exist below the central basin sill, which are shown in Fig. 7. Five profiles, all taken around the easternmost ridge in the central basin (the stations northeast of SL11, see Figs. 2 or 4 for location) are 0.05°C warmer and 0.02 fresher than the rest of the

central basin profiles. This difference is also evident in Figs. 4b and 4c by the sharply dipping isohalines and isopycnals west of Hook Ridge.

b. East basin

Gordon and Nowlin (1978) described central basin stratification as being more complex than that in the east basin. Although the central basin is obviously more stratified than the east basin, the east basin clearly has a more complex stratification. While there are two types of T – S curves present in the central basin (Fig. 6), these merge at the eastern sill depth ($\sigma_1 > 32.56$) into one curve. In contrast, the east basin data do not lie along a single T – S curve despite their greater depth. This inhomogeneity is partially due to complicated topography within the east basin, which comprises three small basins isolated below ~ 2000 m.

These differences between the central and east basin hydrography strongly affect the ability to detect hydrothermal temperature anomalies. While hydrothermal temperature anomalies have been observed in the central basin, it is obvious from Fig. 6 that the lack of a unique T – S curve in the east basin will mask such features. This situation is similar to the Lucky Strike segment of the northern MAR (Wilson et al. 1995) and highlights the importance of using chemical tracers in searching for hydrothermal sources within the east basin.

Shown in Fig. 8 is the T – S diagram for the east basin data. Overlain on Fig. 8a is a T – S curve from the central basin (SL11) for reference and four end-members that could produce east basin bottom water: central basin sill water, Weddell Sea sill water, central basin bottom water, and Weddell Sea bottom water. Figure 8b is an enlargement of the deepest data.

1) CENTRAL BASIN SILL WATER

One of the end-members contributing to east basin bottom water is clearly water above the sill between the central and east basins. This input is apparent in Fig. 8b by the sharp kinks in the east basin T – S curves near the $\sigma_1 = 32.55$ isopycnal. Profiles from SL7, SL8, and SL9 turn abruptly toward the central basin T – S data following lines of constant σ_1 . Each of these profiles is the deepest profile within its subbasin. The input of central basin sill water into the east basin is also implied by the pool of cold, dense water in the westernmost subbasin ($\sim 56.2^\circ\text{W}$) in Fig. 4. This pool is visible on the potential temperature and potential density sections as the -1.2°C isotherm and the $\sigma_2 = 32.55$ isopycnal, which are absent in the east basin outside of this depression. These water properties are similar to the water found just above the sill depth (600–800 m) and suggest that central basin water has spilled over the sill and settled into the deepest parts of each subbasin.

Due to sparse coverage of the east basin by previous investigators this input has not been seen before. Clowes

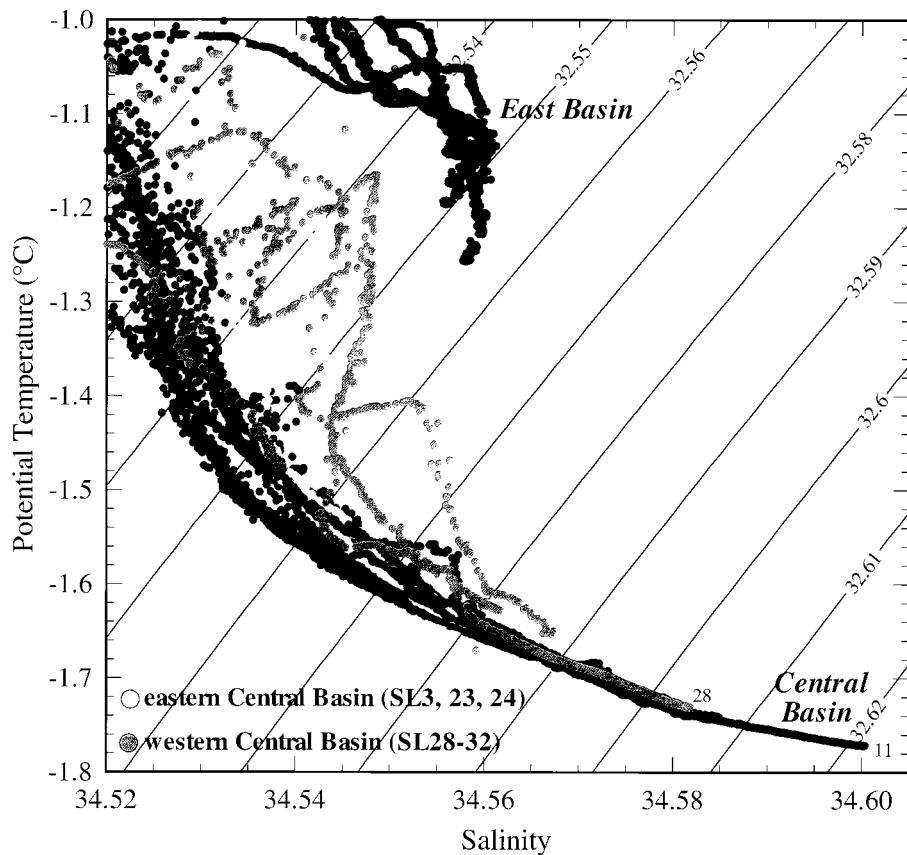


FIG. 6. Potential temperature–salinity diagrams for the deep portion of the central and east basins. Anomalous data from the eastern and western central basin are in gray, the central central basin and the east basin are in black. Lines of σ_1 are shown. The central basin data have a wide depth span relative to the east basin data. As seen in Fig. 4a, the -1.0°C isotherm varies from ~ 300 m in the western central basin to 1400 m in the east basin.

(1934) did not discuss the east basin. The two east basin stations in Gordon and Nowlin (1978) were both within the westernmost subbasin and they assumed that the topographic high at 56°W did not isolate the east basin. However, multibeam data (Gràcia et al. 1996; L. Lawson 1995, personal communication) clearly indicate that waters below 1900 m in the east basin are isolated by this topographic high.

There are three mechanisms that can physically explain the spillover of central basin sill water into the east basin. Creation of central basin bottom water must, by mass conservation, be balanced by an outflow of water. This outflow would occur at the deepest passage out of the central basin, which is the sill into the east basin. Second, hydrothermal activity within the central basin (Schlosser et al. 1988; Chin et al. 1996) could act as a basin pump (Gargett 1988). Gargett (1988) calculated that vertical upwelling resulting from geothermal heating was vigorous enough to drive the observed water influx into the Panama basin, a basin two orders of magnitude larger than the central basin. Third, wind-driven circulation changes could

drive water across the sill into the east basin. These three different mechanisms are not mutually exclusive. Current data from the sill separating the central and east basins are essential to assess the magnitude, variability, and origins of this process.

2) WEDDELL SEA SILL WATER

There must be an input of relatively warm, fresh water into the east basin that does not contribute to central basin waters. A significant difference between the two basins is that the east basin is not isolated below 500 m, as seen in Fig. 2a. Sills of 700–800 m provide access to warmer Weddell Sea water, which could be one component of east basin deep water. Temperature and salinity of NODC data from the southern passage into the east basin (62°S , 54.2°W) were taken to represent the Weddell Sea sill water end-member, which, as seen in Fig. 8a, is considerably warmer and fresher than most central basin deep water. Below the $\sigma_2 = 32.5$ isopycnal (500–600 m) data from the central and eastern subba-

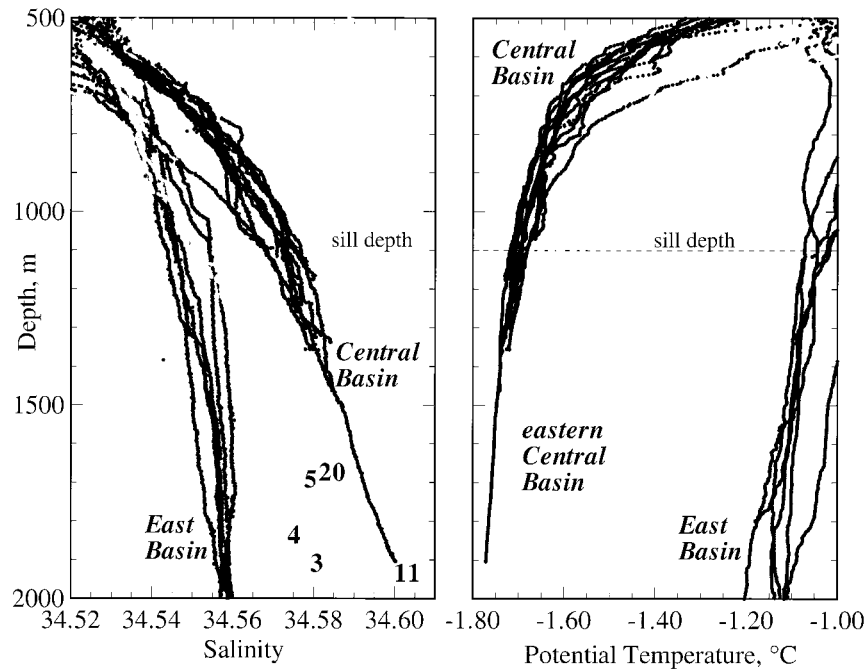


FIG. 7. Profiles of potential temperature and salinity within the central and east basins. Stations from the eastern part of the central basin, marked in gray, are fresher and warmer than the rest of the central basin data. The dashed line at 1100 m marks the maximum depth of the sill between the central and east basins.

sins, the closest to the passage into the Weddell Sea, approach the Weddell Sea sill end-member (Fig. 8a). This observation supports the supposition that water from the Weddell Sea sill contributes to the makeup of the east basin bottom water.

3) CENTRAL BASIN AND WEDDELL SEA DEEP WATER

It is clear from Fig. 8a that east basin deep water is not simply a mixture of central basin sill water and

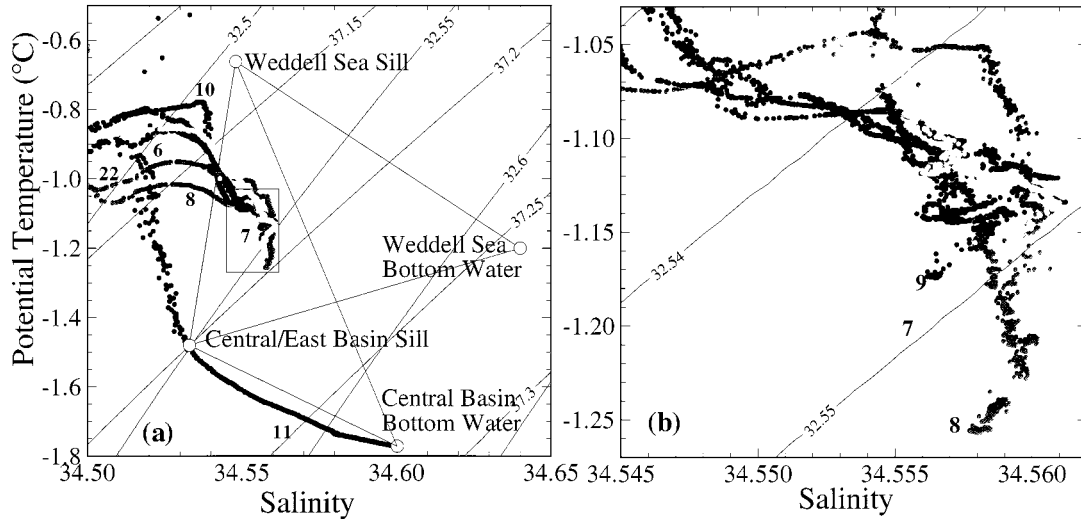


FIG. 8. Potential temperature–salinity diagram of the six east basin stations. Data from the western subbasin are shown in dark gray, the central subbasin in lighter gray, and the eastern subbasin in black. The data can be expressed as a ternary mixture between Weddell Sea sill water, central basin sill water, and central basin bottom water or Weddell Sea bottom water. SL11 from the central basin is shown for reference. (b) T – S diagram of the deepest data outlined in (a) by the boxed area. Lines of constant σ_1 and σ_2 are overlaid on (a), and lines of σ_1 are on (b).

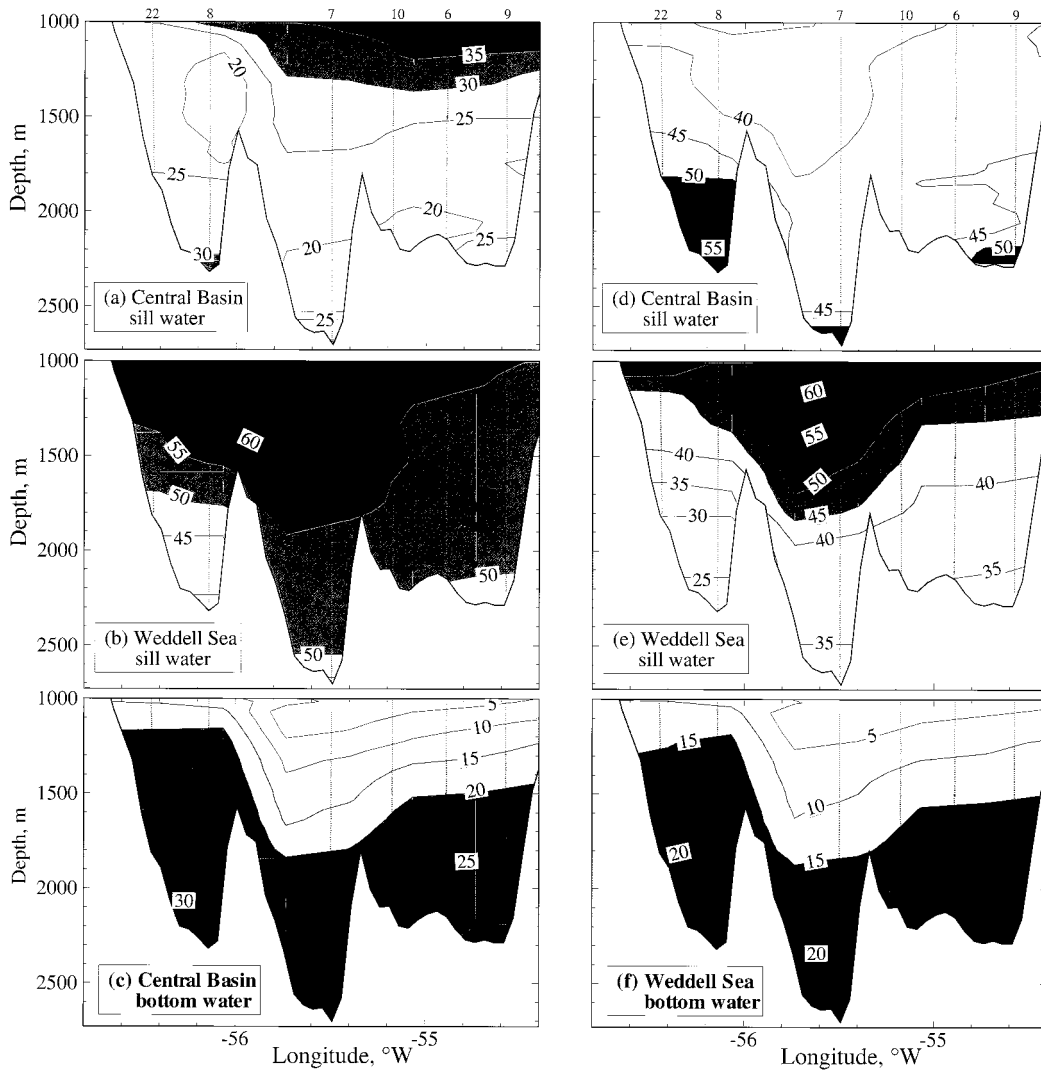


FIG. 9. Contour diagrams showing the proportion and distribution within the east basin of four end-member water masses. Proportions were calculated from a ternary mixture of central basin sill water, Weddell Sea sill water, and central basin bottom water (a)–(c) and from a ternary mixture of central basin sill water, Weddell Sea sill water, and Weddell Sea bottom water (d)–(f).

Weddell Sea sill water—there must be another saltier component. Central basin bottom water and Weddell Sea bottom water (Carmack 1977; Whitworth et al. 1994) both have appropriate T – S properties to be the additional end-member. Neither of these water masses can directly enter the east basin due to topographical barriers; however, both water masses are formed by convection of surface water that could enter into the east basin. While both probably contribute to east basin bottom water, a third variable is needed to fully resolve this question. In an attempt to constrain this problem, proportions of the four end-members within the east basin were calculated using two ternary mixtures: one with central basin bottom water and one with Weddell Sea bottom

water. In both calculations, central basin sill water and Weddell Sea sill water were the other two end-members.

Shown in Fig. 9 are contours of end-member proportions from the two ternary calculations. The biggest difference between using central basin bottom water as an end-member (Figs. 9a–c) versus Weddell Sea bottom water (Figs. 9d–f) is in the distributions of central basin sill water shown in Figs. 9a and 9d. In Fig. 9a the maximum percentage of dense central basin sill water is in the upper (1000–1800 m) eastern half of the east basin and actually decreases toward the central basin sill. In contrast, the distribution of central basin sill water in Fig. 9d is greatest in the deepest portions of each subbasin and is fairly uniform in the upper portion

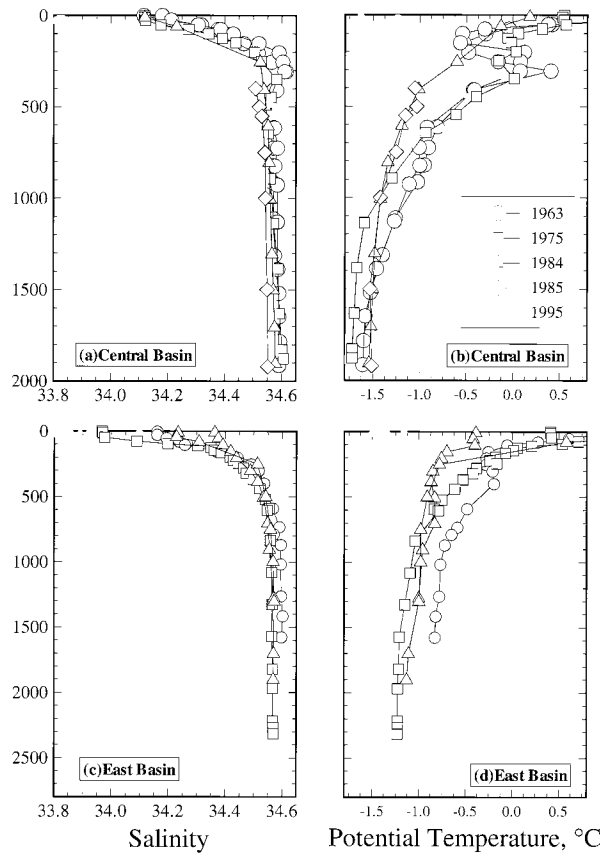


FIG. 10. Profiles of potential temperature and salinity from 1963 (circles), 1975 (squares), 1984 (triangles), 1985 (diamonds), and 1995 (gray lines) for the central and east basins. All of the east basin stations from 1995 are shown, while for the central basin only SL3 and SL11 are shown.

of the basin outside of a minimum in the middle of the basin, which is the result of a strong input of Weddell Sea sill water. Thus, the distribution generated by the ternary mixture ensemble with Weddell Sea bottom water is more plausible. While central basin bottom water cannot be ruled out as contributing to east basin bottom water, this analysis suggests that Weddell Sea bottom water has a greater influence. As seen in Figs. 9c and 9f, neither of these end-members, taken separately, contribute more than 30% to the east basin bottom water. In reality, the proportion shown for one end-member is probably shared between these two end-members.

The predominate end-member of the east basin deep water is Weddell Sea sill water (Figs. 9b and 9d). Its overall distribution is unaltered by the choice of a deep end-member, though its relative proportion increases by 10%–15% when Weddell Sea bottom water is used rather than central basin bottom water. In either case, Weddell Sea sill water contributes more than 40% throughout the entire upper portion, with a maximum of 60% in the central portion of the east basin, coincident with the location of the passage into the Weddell Sea.

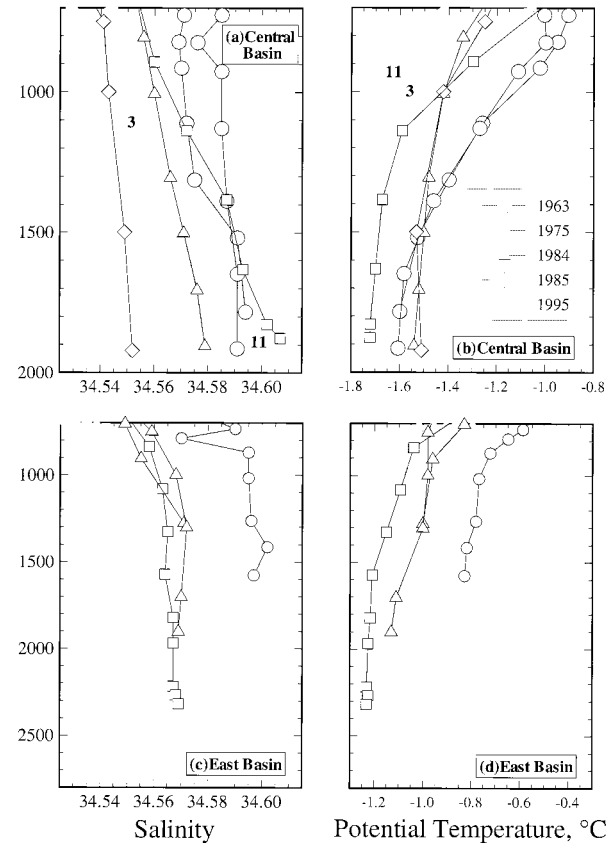


FIG. 11. Profiles, below 700 m, of potential temperature and salinity from 1963 (circles), 1975 (squares), 1984 (triangles), 1985 (diamonds), and 1995 (gray lines) for the central and east basins. All east basin stations from 1995 are shown, while for the central basin only 1995 SL3 and SL11 are shown.

An important caveat is that there is probably significant variability in each of the end-members in the above calculation, and that the dominant end-member, Weddell Sea sill water, probably has the largest associated uncertainty. The Weddell Sea sill water T - S properties are based on a 1976 station in the NODC dataset, and it is likely that these properties were different in 1995. Ideally the calculation should be made with concurrent data from all possible sources to the east basin deep water. However, despite the absence of such data, this study has made a preliminary estimation of the composition of east basin deep water that can be further clarified with future investigations.

c. Temporal variability

The residence time for the Bransfield water, which is on the order of 30 years (Schlosser et al. 1988), is extremely short by deep ocean standards and allows the possibility of temporal variability over a measurable timescale. Gordon and Nowlin (1978) briefly discussed the temporal variability within the Bransfield water,

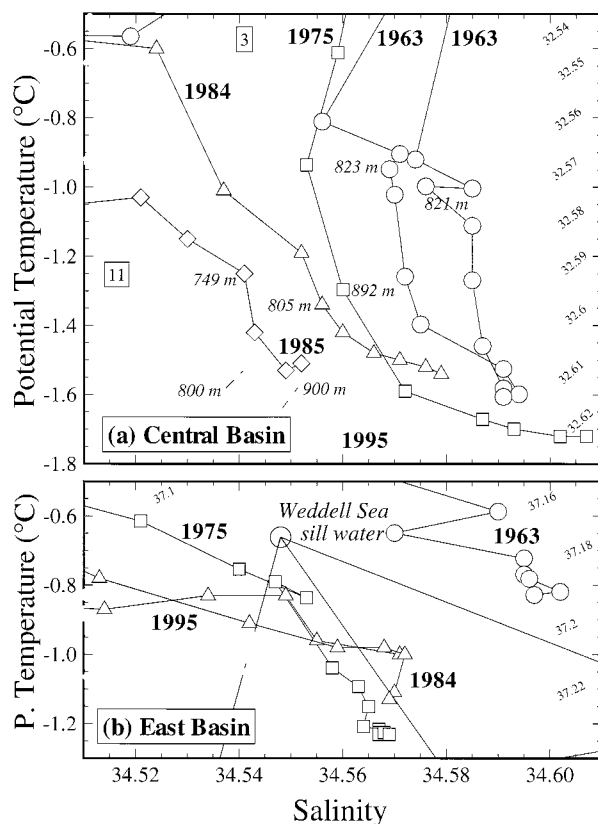


FIG. 12. Potential temperature versus salinity for data from 1963 (circles), 1975 (squares), 1984 (triangles), 1985 (diamonds), and 1995 (gray dots) for (a) the central and (b) the east basin. The depths of some of the data points are given in italics. The solid lines in (b) are the lines that connect the four T - S end-members as shown in Fig. 8a. Lines of constant σ_1 and σ_2 are overlain on (a) and (b), respectively.

comparing their 1975 data from the central and east basins to 1963 data from the USNS *Eltanin* (Friedman 1964) and to data from 1929 and 1932 from Clowes (1934). Here we extend that study by examining these same datasets (except the Clowes data) in addition to data from 1984 and 1985 (Schlosser et al. 1988) and our 1995 data. All the data are from within the same three-month span (Nov–Jan), except for the 1975 data which were collected slightly later in February and March. This information is summarized in Table 1.

In Fig. 10 temperature and salinity profiles from the *Palmer* cruise (1995) are shown alongside the historic data. The surface water (0–300 m) of the central and

east basins in 1995 was colder and fresher than any previous measurements although there is no seasonal difference in the times the measurements were taken. The surface water in 1995 was 1°C colder than in previous years in both basins. The central basin surface water was fresher by about 0.2 in 1995, while in the east basin the historical data overlaps with the saltiest of the 1995 profiles. The CDW was present in the central basin in 1963 and to a lesser extent in 1975. It was only seen in the east basin in 1963, although the temperature maximum was much less pronounced than was seen in 1995.

Changes in the temperature and salinity of the deep water are easier to see on the profiles below 700 m shown in Fig. 11. Central basin deep water was colder in 1995 than any measurement in the last 30 years. However, the deep water has not been steadily losing heat, evidenced by the warming between 1975 and 1985. The deep salinity has remained fairly constant, except for in 1984 and 1985, when there were considerably fresher salinities. However, there is likely a geographic element to these fresher salinities as these data were east of the 1995 SL11 (see Fig. 2b), and thus in the region where fresher salinities were also observed in 1995 (Fig. 7). The bottom 1984 salinity is virtually identical to 1995 data from the same area (SL3), while the 1985 data are fresher by 0.03.

Figure 12 is a T - S plot of the historic data and some of the 1995 data. Over the 30-yr time span the slope of the central basin T - S relation has undergone a systematic change. The water above the sill (750–900 m) has steadily become colder and fresher, while the bottom water has remained relatively constant, resulting in a change from the nearly vertical T - S relationship in 1963 to the nearly horizontal one in 1995.

Changes in east basin bottom water over the last 30 years differ from those observed in the central basin. Like the central basin, the east basin has become colder and fresher in the past 30 years, however, the general slope of the east basin T - S relation has remained constant (Fig. 12b). Also in contrast to the central basin, the T - S changes in the east basin have been more sporadic. The most dramatic salinity and temperature decrease, 0.04° and 0.3°C, occurred between 1963 and 1975, while the greatest change between either 1975 and 1984 or 1984 and 1995 is less than half this magnitude.

The heat and freshwater fluxes associated with the observed temporal changes in temperature and salinity

TABLE 1. Information on the historical data used.

Date	Ship	Reference	Data source
Jan 1963	<i>Eltanin</i>	Friedman (1964)	NODC
Feb–Mar 1975	<i>Conrad, Melville</i>	Gordon and Nowlin (1978)	NODC
Nov 1984–Jan 1985	<i>Polarstern</i>	Schlosser et al. (1988)	Reference
Nov 1985	<i>Polarstern</i>	Schlosser et al. (1988)	Reference
Nov 1995	<i>N.B. Palmer</i>	This work	This work

TABLE 2. Heat and freshwater fluxes below 1000 m for the central basin (CB) and the east basin (EB) using an average depth of 1700 and 2200 m, respectively. The calculation was done twice for the 1984–95 period in the central basin using SL11 and SL3. The east basin calculation used an average of the 1995 data.

Period	Heat flux (W m^{-2})			Freshwater input (m m^{-2})		
	CB	EB	CB + EB	CB	EB	CB + EB
1963–75	−1.47	−4.97	−5.44	+0.05	+0.60	+0.65
1975–84	+1.69	+2.15	+3.84	+0.45	−0.12	+0.33
1984–95	−1.67 (3) −2.03 (11)	+1.76 (3) −0.27	+1.76 (3) −2.3 (11)	+0.08 (3) −0.31 (11)	+0.41	+0.49 (3) +0.10 (11)
1963–95	−1.45 (3) −1.81 (11)	−3.09	−4.54 (3) −4.90 (11)	+0.58 (3) +0.19 (11)	+0.89	+1.47 (3) +1.08 (11)

are shown in Table 2. The freshwater flux for the 1975–84 period in the central basin is overestimated because the lower salinity of the 1984 data is likely influenced by geographical factors. The same is true for SL3 from 1995; thus two calculations were made for the 1984–95 time period in the central basin, one for each of the two different 1995 profiles (SL3 and SL11). The calculation using SL3 should be more accurate as this station was in the same area as the 1984 profile (see Fig. 2). However, for the net flux calculation (1963–95) SL11 should be used as it is outside of the anomalous low salinity area. The net heat flux and freshwater flux were both greater in the east basin than the central basin. The most significant proportion of the east basin fluxes occurred between 1963 to 1975. The combined fluxes for both basins over the 32-yr time period are equal to a heat loss of 4.9 W m^{-2} and a freshwater input of 1.1 m m^{-2} .

The warm salty water observed in the east basin in 1963 is interesting because it lies outside of the ternary mixing diagrams outlined in Fig. 8a. Even using the warmer, saltier properties of 1963 central basin sill water cannot produce the east basin bottom water observed in 1963. To obtain the 1963 T – S values requires that one of the other two end-members, Weddell Sea sill

water or Weddell Sea bottom water, be warmer or saltier than in the model presented here. However, both the 1975 and the 1984 data fall within the proposed mixing triangles (Fig. 8a). End-member proportions were calculated for these data and are shown with SL8 of the 1995 data (SL8 is geographically the closest to the locations of the 1975 and 1984 data) in Fig. 13. The properties of central basin sill water were adjusted to reflect changes observed in this water mass. The end-member proportions calculated for the 1984 data are virtually identical to those of the 1995 data. In 1975 there appeared to be a 20% increase in the proportion of central basin sill water, balanced by a 10% reduction in the amount of Weddell Sea sill water and Weddell Sea deep water. It is not possible to further quantify changes in the end-member compositions of the east basin without knowing the temperature and salinity variability of the sill water and the bottom water of the Weddell Sea over the past 30 years.

5. Conclusions

The CDW has traditionally been described as absent or only weakly present within Bransfield Strait, with an entrance between Smith and Snow Islands in the west.

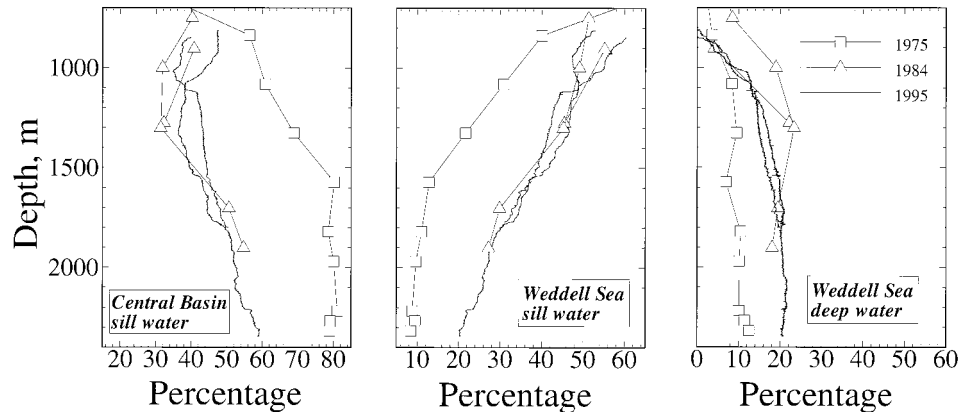


FIG. 13. Profiles of proportions of (a) central basin sill water, (b) Weddell Sea sill water, and (c) Weddell Sea deep water in 1975 (squares), 1984 (triangles), and 1995 (gray lines) in the east basin.

In contrast, during the *Palmer* study in 1995, the CDW extended throughout most of the central basin. At the western part of the central basin the CDW was present as a narrow band near Deception Island with a strong thermal gradient at its southern boundary, consistent with previous observations. The greatest amount of CDW seen within the strait was over the sill connecting the central and east basins.

The waters within the central and east basins have different *T-S* properties and are distinct from the surrounding waters outside of the strait. The central basin bottom water is more stratified than the east basin bottom water but lacks its complexity and can be viewed as the product of a single process. In contrast, the east basin bottom water is clearly a mixture of multiple water masses. A model presented here explains the east basin bottom water as a ternary mixture of central basin sill water, Weddell Sea sill water, Weddell Sea bottom water and/or central basin bottom water. Weddell Sea sill water is the predominate end-member, constituting 40%–60% throughout most of the deep east basin. Central basin bottom water and Weddell Sea bottom water together contribute less than a third within the deepest parts of the subbasins, with Weddell Sea bottom water probably dominating this component. Central basin sill water contributes the most to the deep subbasins, where it reaches 50%.

Temperature and salinities within the central and east basins of Bransfield strait have varied considerably over the past 30 years. A systematic change in the slope of the *T-S* relation in the central basin is observed, the result of the middepth water becoming colder and fresher. The deep water of the east basin has also cooled and freshened but uniformly throughout the water column without a change in the *T-S* slope. Changes in the east basin have been temporally sporadic, with the largest change occurring between 1963 and 1975.

Acknowledgments. This work was part of the Ph.D. thesis of the first author and was supported by Grant OPP-9317361 to GPK. Thanks to the captain and crew of the RVIB *Nathaniel B. Palmer* and to Larry Lawver, the chief scientist. We also thank Bob Collier, Rick Thomson, Andrew Bennett, and two anonymous reviewers for comments that improved this paper. The maps were made using GMT software (Wessel and Smith 1991).

REFERENCES

- Baker, P. E., and I. McReath, 1971: 1970 eruption at Deception Island. *Nature*, **231**, 5–9.
- , T. G. Davies, and M. J. Roobol, 1969: Volcanic activity at Deception Island in 1967 and 1969. *Nature*, **224**, 553–560.
- Birkenmajer, K., and R. A. Keller, 1990: Pleistocene age of the Melville Peak volcano, King George Island, West Antarctica, by K-Ar dating. *Bull. Polish Acad. Sci. Earth Sci.*, **38**, 17–24.
- Brault, M., and B. R. T. Simoneit, 1990: Mild hydrothermal alteration of immature organic matter in sediments from the Bransfield Strait, Antarctica. *Appl. Geochem.*, **5**, 149–158.
- Capella, J. E., L. B. Quetin, E. E. Hofmann, and R. M. Ross, 1992a: Models of the early life history of *Euphausia superba*—Part II. Langrangian calculations. *Deep-Sea Res.*, **39**, 1201–1220.
- , R. M. Ross, L. B. Quetin, and E. E. Hofmann, 1992b: A note on the thermal structure of the upper ocean in the Bransfield Strait–South Shetland Islands region. *Deep-Sea Res.*, **39**, 1221–1229.
- Carmack, E. C., 1977: Water characteristics of the Southern Ocean south of the Polar Front. *Voyage of Discovery*, M. Angel, Ed. Pergamon, 15–41.
- Chin, C. S., G. P. Klinkhammer, C. Wilson, L. A. Lawver, and J. Lupton, 1996: Hydrothermal activity in a nascent backarc basin: the Bransfield Strait, Antarctica (abstract). *Eos Trans. Amer. Geophys. Union*, **77**, F413.
- Clowes, A. J., 1934: Hydrology of the Bransfield Strait. *Discovery Rep.*, **9**, 1–64.
- Elderfield, H., 1972: The effects of volcanism on seawater chemistry, Deception Island, Antarctica. *Mar. Geol.*, **13**, M1–M6.
- Friedman, S. B., 1964: Physical oceanography data obtained during *Eltanin* cruises 4, 5 and 6 in the Drake Passage, along the Chilean coast and in the Bransfield Strait, June 1962–January 1963, LDGO Tech. Rep. 1, CU-1–64, 55pp.
- Gargett, A., 1988: Is the thermohaline circulation “pushed” or “pulled”? *Ocean Modelling* (unpublished manuscripts), **78**, 10–14.
- Gordon, A. L., 1967: Structure of Antarctica waters between 20°W and 170°W. *Antarct. Map Folio Series*, V. Bushnell, Ed., Vol. 6 Amer. Geogr. Soc., 14 pp.
- , and W. D. J. Nowlin, 1978: The basin waters of the Bransfield Strait. *J. Phys. Oceanogr.*, **8**, 258–264.
- Gràcia, E., M. Canals, M. Farràn, M. J. Prieto, J. Sorribas, and GE-BRA Team, 1996: Morphostructure and evolution of the Central and Eastern Bransfield Basins (NW Antarctic Peninsula). *Mar. Geophys. Res.*, **18**, 429–448.
- Grelowski, A., and R. Tokarczyk, 1985: Hydrological conditions in the region of Bransfield Strait and southern part of Drake Passage in the period from December 10, 1983 and January 8, 1984 (BIOMASS-SIBEX). *Polish Polar Res.*, **6**, 31–41.
- Hofmann, E. E., J. E. Capella, R. M. Ross, and L. B. Quetin, 1992: Models of the early life history of *Euphausia superba*—Part I. Time and temperature dependence during the descent–ascent cycle. *Deep-Sea Res.*, **39**, 1177–1200.
- , J. M. Klinck, C. M. Lascara, and D. A. Smith, 1996: Water mass distribution and circulation west of the Antarctic Peninsula and including Bransfield Basin. *Foundations for Ecological Research West of the Antarctic Peninsula*, Antarctic Research Series, Vol. 70, 61–800.
- Huntley, M., D. M. Karl, P. P. Niiler, and O. H. Holm-Hansen, 1991: Research on Antarctica Coastal Ecosystem Rates (RACER): an interdisciplinary field experiment. *Deep-Sea Res.*, **38**, 911–941.
- Keller, R. A., M. R. Fisk, W. M. White, and K. Birkenmajer, 1992: Isotopic and trace element constraints on mixing and melting models of marginal basin volcanism, Bransfield Strait, Antarctica. *Earth Planet. Sci. Lett.*, **111**, 287–303.
- Killworth, P. D., 1983: Deep convection in the world ocean. *Rev. Geophys. Space Phys.*, **21**, 1–26.
- Lawver, L. A., B. J. Sloan, D. H. N. Barker, M. Ghidella, R. P. Von Herzen, R. A. Keller, G. P. Klinkhammer, and C. S. Chin, 1996: Distributed, active extension in Bransfield Basin, Antarctic Peninsula: Evidence from multibeam bathymetry. *GSA Today*, **6**, 1–6.
- Niiler, P. P., A. Amos, and J.-H. Hu, 1991: Water masses and 200 m relative geostrophic circulation in the western Bransfield Strait region. *Deep-Sea Res.*, **38**, 943–959.
- Orheim, O., 1972: Volcanic activity on Deception Island, South Shetland Islands. *Antarctic Geology and Geophysics*, R. J. Adie, Ed., Universitetsforlaget, 117–130.
- Read, J. F., R. T. Pollard, A. I. Morrison, and C. Symon, 1995: On

- the southerly extent of the Antarctic Circumpolar Current in the southeast Pacific. *Deep-Sea Res. II*, **42**, 933–954.
- Schlosser, P., E. Suess, R. Bayer, and M. Rhein, 1988: ^3He in the Bransfield Strait waters: indication for local injection from back-arc rifting. *Deep-Sea Res.*, **35**, 1919–1935.
- Sievers, H. A., 1982: Descripcion de las condiciones oceanograficas fisicas, como apoya al estudio de la distribucion y comportamiento del krill. Instituto Antartico Chileno, Scientific Series Vol. 28, 87–136.
- , and W. D. Nowlin, 1984: The stratification and water masses at Drake Passage. *J. Geophys. Res.*, **89**, 10 489–10 514.
- Wessel, P., and W. H. F. Smith, 1991: Free software helps map and display data. *Eos, Trans. Amer. Geophys. Union*, **72**, 441, 445–446.
- Whiticar, M. J., and E. Suess, 1990: Hydrothermal hydrocarbon gases in the sediments of the King George Basin, Bransfield Strait, Antarctica. *Appl. Geochem.*, **5**, 135–147.
- Whitworth, T., W. D. Nowlin, A. H. Orsi, R. A. Locarnini, and S. G. Smith, 1994: Weddell Sea shelf water in the Bransfield Strait and Weddell–Scotia Confluence. *Deep-Sea Res.*, **41**, 629–641.
- Wilson, C., K. Speer, J.-L. Charlou, H. Bougault, and G. P. Klinkhammer, 1995: Hydrography above the Mid-Atlantic Ridge (33° – 40°N) and within the Lucky Strike segment. *J. Geophys. Res.*, **100**, 20 555–20 564.